

Surface-plasmon polariton resonances in triangular-groove metal gratings

T. Søndergaard*

Department of Physics and Nanotechnology, Aalborg University, Skjernvej 4A, DK-9220 Aalborg Øst, Denmark

Sergey I. Bozhevolnyi

Institute of Sensors, Signals and Electrotechnics (SENSE), University of Southern Denmark, Niels Bohrs Allé 1, DK-5230 Odense M, Denmark

(Received 3 August 2009; published 5 November 2009)

Electromagnetic resonances of triangular-groove gold gratings illuminated with monochromatic light are studied theoretically. The calculations performed are based on the Green's-function surface-integral equation method with the periodic Green's function. Local-field-enhancement spectra and near-field calculations reveal three types of resonances, namely, geometric resonances determined by the shape of individual grooves, standing-wave surface-plasmon polariton (SPP) resonances due to SPPs reflected by the neighbor grooves, and very sharp resonances (Rayleigh anomalies) at wavelengths near the cutoff wavelength of higher grating-reflection orders, which can be tuned simply by changing the angle of incident light. These resonances are also found to be observable in the reflection spectra, whose minima correspond to peaks in the enhancement spectra. Typical enhancements of the electric field magnitude inside the grooves are larger than 20, reaching in some cases the level of ~ 35 . In the case of Rayleigh anomalies, the total reflection can be almost completely suppressed. The resonances can be realized in the wavelength range from visible to infrared by varying the groove height, angle, and periodicity, a feature that makes this configuration promising for a wide range of practical applications, for example, within surface-enhanced spectroscopies.

DOI: [10.1103/PhysRevB.80.195407](https://doi.org/10.1103/PhysRevB.80.195407)

PACS number(s): 73.20.Mf, 71.36.+c, 42.79.Dj, 02.70.Pt

I. INTRODUCTION

Gratings with a periodic arrangement of grooves or surface scatterers on a metal surface (or metal film) have several applications in the field of plasmonics.^{1,2} Electromagnetic waves known as surface-plasmon polaritons (SPPs) being bound to and propagating along metal surfaces are in this field used for, e.g., signal transportation or for generation of large local electric fields useful for sensing applications. A finite-length grating can be used as a component for the excitation of SPP waves.^{3–8} Alternatively, such gratings can work as band-gap structures for SPP waves such that only SPP waves with certain wavelengths are reflected or filtered away.^{9–11} Grooves in a metal film or surface have also attracted a lot of interest for the enhancing of transmission through subwavelength apertures.^{12,13} Triangular-shaped (V-) grooves that are considered in this paper have been used as optical waveguides with SPP modes, channel plasmon polaritons, being confined to and propagating along the grooves.^{14–17} Such waveguides have been used for the realization of compact photonic components, e.g., a ring resonator.¹⁴ Triangular grooves have been most often fabricated by focused-ion-beam milling¹⁴ but similar waveguides have also recently been fabricated with the nanoimprinting technique.¹⁸

This paper is devoted to detailed theoretical investigations of the resonant behavior of triangular-groove gold gratings. By varying the geometry of grooves and grating period, the angle of incident light, and by calculating optical near fields at resonance, we identify three types of resonances, namely, standing-wave resonances related to SPP waves propagating back and forth between the neighbor grooves, geometric groove resonances related to the shape of individual grooves, and very sharp resonances associated with Rayleigh anomalies.

It is known that the Rayleigh anomalies (or Wood's anomalies) can occur due to the emergence of a new spectral order at grazing angle and, depending on the system configuration, related to guided waves propagating along the grating surface.^{19,20} For example, this type of resonance has been recently observed in the form of extremely narrow reflection minima (few-nanometer spectral width) for two-dimensional (2D) arrays of metallic particles.²¹ Local geometric groove resonances for rectangular-groove (or lamellar) gratings have been observed experimentally in reflection spectra.^{22,23} Resonances due to SPP waves being reflected back and forth between two grooves (of a different shape than ours) were recently observed using cathodoluminescence.²⁴ Standing-wave resonances have also attracted attention for other structures in the field of plasmonics in the form of optical antennas^{25,26} or optical resonators based on metal nanostrips (see, e.g., Refs. 27–29) and metal nanorods (see, e.g., Refs. 30–33).

The paper is organized as follows. In Sec. II the surface-integral equation method used to obtain the results presented in the paper is briefly presented. In Sec. III we investigate how resonances in the local-field-enhancement spectra depend on the geometry of triangular-groove gold gratings. Influence of the angle of light incidence on the spectral position of resonances is investigated in Sec. IV. We demonstrate in Sec. V that, for the SPP standing-wave resonances, structures differing only in the period by an integer number of half-SPP wavelengths (at resonance) exhibit the same resonance wavelength. Reflection spectra are considered in Sec. VI, and finally we offer our conclusions in Sec. VII.

II. NUMERICAL METHOD

The numerical results presented throughout the paper have all been obtained with the Green's-function surface-

integral equation method with the periodic Green's function. We consider a 2D geometry. Along the third direction (z) the structure and the fields are assumed invariant. In the case of p -polarized light the magnetic field then only has a z component, i.e., $\mathbf{H}(x, y) = \hat{z}H(x, y)$, where \hat{z} is a unit vector along the z axis. The grating we will consider is a periodic structure (along x) consisting of a planar gold surface with periodically spaced triangular indentations and air above the grating. The magnetic field at a position \mathbf{r} in the air region above the grating is related to the magnetic field and its normal derivative at the grating surface via the following integral over one period of the metal-air interface:

$$H(\mathbf{r}) = H_0(\mathbf{r}) + \int_{1 \text{ period}} [H(\mathbf{s}') \hat{n}' \cdot \nabla' g_{air}(\mathbf{r}, \mathbf{s}') - g_{air}(\mathbf{r}, \mathbf{s}') \hat{n}' \cdot \nabla' H_{air}(\mathbf{s}')] dl', \quad (1)$$

where \hat{n} is the surface-normal vector pointing into the air region, $H_0(\mathbf{r}) = A e^{-ik_x x} e^{iky y} (e^{i\omega t})$ is the incident plane wave satisfying $(\nabla^2 + k_0^2 \epsilon_{air}) H_0(\mathbf{r}) = 0$ with the free-space wave number k_0 and dielectric constant of air $\epsilon_{air} = 1$, and g_{air} is the free-space periodic Green's function. H_{air} instead of H means that we should use the magnetic field on the air side of the interface.

For positions in the metal region the magnetic field at a position \mathbf{r} is instead given by

$$H(\mathbf{r}) = - \int_{1 \text{ period}} \left[H(\mathbf{s}') \hat{n}' \cdot \nabla' g_m(\mathbf{r}, \mathbf{s}') - g_m(\mathbf{r}, \mathbf{s}') \frac{\epsilon_m}{\epsilon_{air}} \hat{n}' \cdot \nabla' H_{air}(\mathbf{s}') \right] dl', \quad (2)$$

where g_m is the periodic Green's function of a homogeneous metal and ϵ_m is the complex dielectric constant of the metal. We obtain ϵ_m for gold by linear interpolation of the Johnson and Christy data³⁴ to the wavelength of interest. There is no incident field in the latter equation because the field is incident on the grating from the air side. Self-consistent equations for the magnetic field and its normal derivative are obtained by letting the position \mathbf{r} approach the surface from either side. The resulting equations are discretized and the field in each (possibly slightly curved) surface element is assumed constant. This results in a matrix equation for the discretized field and normal derivative that can be solved on a computer. Once the field and its normal derivative are known at the surface the field can be calculated at all other positions using the above two equations. We calculate the electric field from the magnetic field $[\mathbf{E} = (\nabla \times \mathbf{H}) / i\omega \epsilon]$, which means when we use Eqs. (1) and (2) we have to calculate double derivatives of the Green's function.

The periodic Green's function is given by

$$g_{air(m)}(\mathbf{r}, \mathbf{r}') = - \frac{i}{22\pi} e^{-ik_x(x-x')} \sum_n e^{inG(x-x')} \frac{e^{-ik_{y,n}|y-y'|}}{k_{y,n}} G, \quad (3)$$

where $G = 2\pi/\Lambda$ with Λ being the period of the grating, k_x is the x component of the wave vector of the incident plane

wave, and $k_{y,n} = \sqrt{k_0^2 \epsilon_{air(m)} - (k_x - nG)^2}$ with $\text{imag}(k_{y,n}) \leq 0$.

This Green's function satisfies the usual equation ($\nabla^2 + k_0^2 \epsilon_{air(m)} g_{air(m)}(\mathbf{r}, \mathbf{r}') = -\delta(\mathbf{r}, \mathbf{r}')$), and with this choice of Green's function the field calculated with Eqs. (1) and (2) will satisfy the radiating boundary condition meaning that except for the component H_0 the field should propagate away from the grating surface. Furthermore, the Green's function satisfies the boundary condition

$$g(x - x' + n\Lambda, y - y') = g(x - x', y - y') e^{-ik_x n\Lambda}. \quad (4)$$

The total field will be a Bloch wave with the Bloch-wave number k_x . In the calculations all corners are rounded with a bending radius of 2 nm. The method is very similar to the surface-integral equation method presented in Refs. 35–37 except that it has been modified to the case of periodic structures by replacing the usual Green's function with the periodic Green's function,^{38,39} and the fact that we do not integrate over a closed surface but one period of a periodic structure. The integral over the missing part of the closed surface accounts for the term H_0 [Eq. (1)] or vanishes [Eq. (2)].

By using a large period we have checked that convergence is similar to our previous work with the usual (nonperiodic) Green's function³⁵ and we can reproduce the same analytical results,³⁵ the same numerical results by other authors (in which case rounding of sharp corners can be important for the convergence),³⁵ and numerical results being in agreement with experiments.²⁸ Furthermore, the method has been validated by comparing calculations for a range of periodic surface profiles with similar calculations based on the area and volume Green's-function integral equation methods³⁵ with a periodic Green's function, and a very simple check has been to model layered media as a periodic structure in which case we have compared with analytical results.

III. GROOVE GEOMETRY

The structure we are interested in is a grating characterized by a periodic arrangement of triangular grooves with height h and groove angle α in a gold surface (inset of Fig. 1). In order to start the analysis with a case where the complexity is as small as possible, we choose a grating period $\Lambda = 500$ nm which is not larger than the considered wavelengths λ ($500 \leq \lambda \leq 1500$ nm) avoiding thereby higher-order reflections for normally incident light.

For the 500-nm-period gratings with the groove height $h = 200$ nm and angles $\alpha = 20^\circ$, 30° , and 40° , we have calculated in a wide range of wavelengths the enhancement of magnitude of the local electric field near the bottom of a groove (24 nm above the groove tip) as compared to the normally incident p -polarized plane wave [Fig. 1(a)]. By using a position which is not exactly at the bottom of the groove we avoid that the result will be sensitive to the choice of rounding used for the corner at the bottom of the groove.

Results are also shown for the case of s -polarized incident light [Fig. 1(b)] to illustrate that the field enhancements achievable with that polarization are very small, especially close to the metal surface, and that there are no resonances in

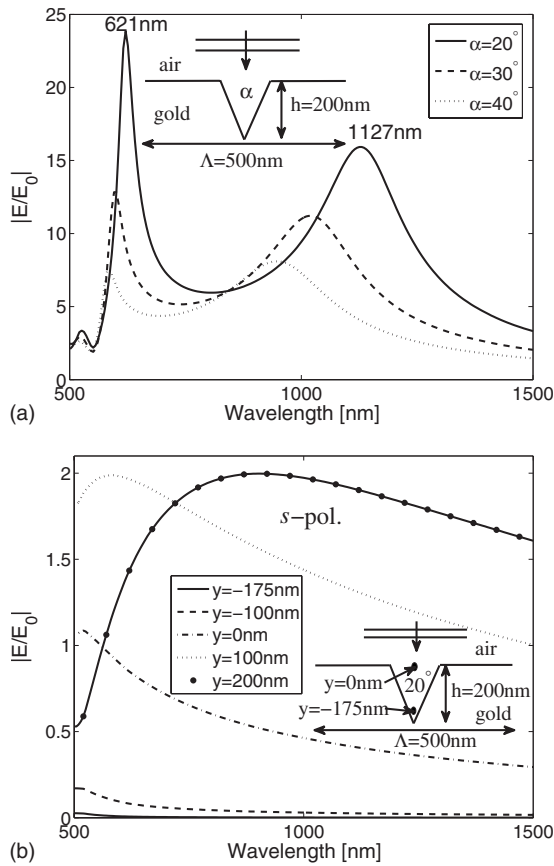


FIG. 1. (a) Enhancement spectra of the electric field magnitude (compared to the normally incident *p*-polarized plane wave) at a position close to the groove bottom of the 500-nm-period grating for different groove angles α (see inset). (b) Enhancement spectra at different positions above the groove bottom for the structure with groove angle $\alpha=20^\circ$ in the case of *s*-polarized light.

the spectra. The highest local-field enhancements of a factor of 2 for *s* polarization [Fig. 1(b)] is similar to the maximum achievable local-field enhancement that would be obtained in the case of a flat metal surface due to interference between the incident and reflected waves. As sharp resonances and large local-field enhancements are not available with *s*-polarized light (at least, in the considered parameter range) we will for the remainder of the paper deal only with *p*-polarized light.

For *p* polarization and all three considered groove angles [Fig. 1(a)] one notices two significant resonance peaks, e.g., at the wavelengths 621 and 1127 nm for the groove angle $\alpha=20^\circ$, whose positions are influenced (blueshifted) albeit to a different degree by increasing the groove angle. The nature of the short-wavelength resonance (621 nm) is revealed from a calculation of the electric near-field distribution around the grooves [Fig. 2(a)] showing that the field to a large extent is localized to a region near the bottom of the groove. We associate this resonance with a geometric resonance of an individual groove occurring due to the field bouncing between the groove top and bottom in a way similar to what takes place in lamellar or rectangular grooves.^{22,23}

The long-wavelength resonance (1127 nm) has a large amount of the field located above the groove [Fig. 2(b)]. In

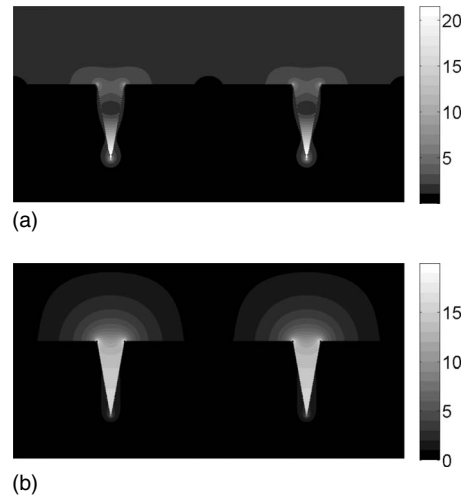


FIG. 2. Normalized electric field magnitude distributions near the 500-nm-period groove grating being illuminated with *p*-polarized light with wavelength (a) 621 nm and (b) 1127 nm. The groove height is 200 nm and the groove angle is $\alpha=20^\circ$.

this case, we hypothesize that the resonance is caused by standing waves related to SPPs propagating back and forth (along the surface) between the neighbor groove bottoms. This hypothesis is supported further throughout the paper by simulations for different angles of incident light and grating periods, including further calculations of the near-field distributions for those cases. Note that the resonant wavelength is close to being two times larger than the groove period, i.e., close to the round-trip distance. It should be of course borne in mind that the reflection phase might depend on the groove angle α and that the precise location where reflection takes place is also not well defined. Note that for the resonators based on short-range SPPs the reflection phase can significantly influence the width of a resonator to be different from half the desired resonance wavelength.²⁸ Standing-wave resonances of a similar nature but for two rectangular grooves have also been observed experimentally.²⁴

If we consider a position with smaller distance to the groove tip we can marginally increase the peak of the short-wavelength resonance but at the expense of a slightly decreased peak at the long-wavelength resonance. Thus we consider the height 25 nm above the groove tip to be a good compromise where both peaks are very near to their maximum.

The maximum physical round-trip distance that one could assume for an SPP to propagate when being reflected back and forth between the neighbor grooves is twice the distance L between the groove bottoms along the surface, where

$$L = \Lambda + 2h\{\sqrt{1 + [\tan(\alpha/2)]^2} - \tan(\alpha/2)\}. \quad (5)$$

Within the assumption of propagation taking place in the form of SPP's the optical path length per round trip will not differ much from $2L$ because the SPP mode index is close to unity. The distance L changes from 835 nm for $\alpha=20^\circ$ to 780 nm for $\alpha=40^\circ$ in accordance with the observed blueshift of the resonance wavelength when increasing the angle α . The resonance wavelength changes from 1127 nm ($\alpha=20^\circ$) to

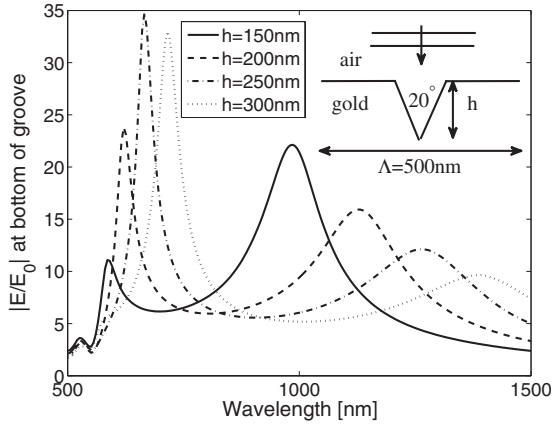


FIG. 3. Enhancement spectra of the electric field magnitude (compared to the normally incident *p*-polarized plane wave) at a position close to the groove bottom of the 500-nm-period grating (see inset) for different groove heights *h*.

950 nm ($\alpha=40^\circ$), i.e., by 187 nm, which is somewhat different from the change in $2L$ (110 nm). The difference can be understood if we consider propagation in the groove to take place in the form of a gap SPP. The larger mode index of a gap SPP results in an increased optical path length and therefore a resonance wavelength which is larger than $2L$. This increase will be higher for $\alpha=20^\circ$ than for $\alpha=40^\circ$ because the gap-SPP mode index increases with decreasing gap width.

In the next step, we consider changing only the groove height *h* for the same geometry as before ($\Lambda=500$ nm, $\alpha=20^\circ$). One notices (Fig. 3) that both the short- and long-wavelength resonance peaks are redshifted with the increase in groove height, features that are consistent with the interpretations suggested for these resonances. For example, the change in height *h* from 150 to 300 nm results in an increase in the round-trip distance $2L:2\Delta L=506$ nm [Eq. (5)]. The corresponding increase in the resonance wavelength constitutes ~ 405 nm (from 985 to 1390 nm), which is at least not far away from $2\Delta L$ (the above remark on the reflection phase is also relevant in this case).

IV. ANGLE OF LIGHT INCIDENCE

The aforementioned interpretations of the short- and long-wavelength resonances seen in Figs. 1–3 implies that these resonances (being determined only by the groove geometry and round-trip distance) should not depend on the angle of light incidence. This is confirmed by considering the angles of incidence $\theta_i=0^\circ, 10^\circ, 20^\circ, 30^\circ$, and 40° (Fig. 4) since the resonance peaks at $\lambda \approx 621$ and 1127 nm appear for all considered angles of incidence.

However, the spectra for the larger angles are more complex due to the appearance of sharp features, “spikes” and/or dips, at a wavelength close to

$$\lambda = \Lambda + \Lambda \sin \theta_i, \tag{6}$$

corresponding to the cutoff wavelength where the first diffraction order in reflection from the grating appears. At this

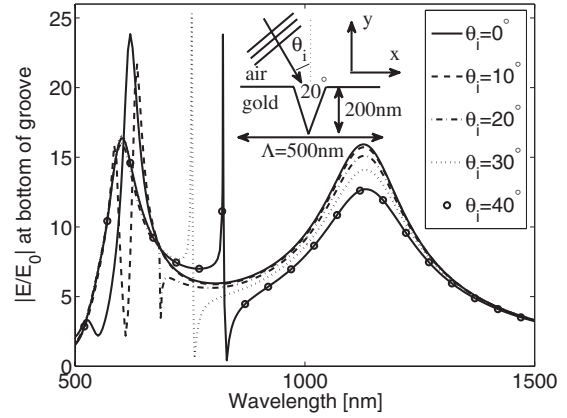


FIG. 4. Enhancement spectra of the electric field magnitude (compared to the incident *p*-polarized plane wave) at a position close to the groove bottom of the 500-nm-period grating for different angles θ_i of light incidence.

precise wavelength the reflected light in the first diffraction order is grazing the grating surface. E.g., for the angle of incidence of 40° , the above formula [Eq. (6)] results in the wavelength of 821.4 nm, and the calculated spike is located at this wavelength within 0.2 nm. At this wavelength, the reflected (in the first diffraction order) light propagates along the negative *x* axis according to the definition of θ_i and the coordinate system in the inset of Fig. 4.

It is instructive to consider the near-field distribution at the wavelength of the spike resonance (Fig. 5). The field distribution just above the grating is relatively featureless, supporting the idea of strong excitation of waves barely grazing the grating surface and propagating only along the negative and not along the positive *x* axis since in that case we would have seen a standing-wave picture.

Note that, for the relatively short period of $\Lambda=500$ nm discussed in so far, higher diffraction orders in reflection were not present in the considered wavelength interval for normally incident light. The field-enhancement spectra become slightly more complicated for larger periods, e.g., for $\Lambda=800$ nm (Fig. 6). In this case we find for normal inci-

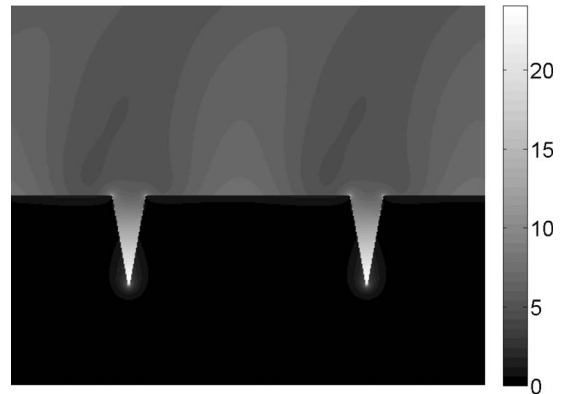


FIG. 5. Normalized electric field magnitude distributions near the 500-nm-period groove grating being illuminated with *p*-polarized light at the wavelength of 821.5 nm. The angle of incidence is $\theta_i=40^\circ$.

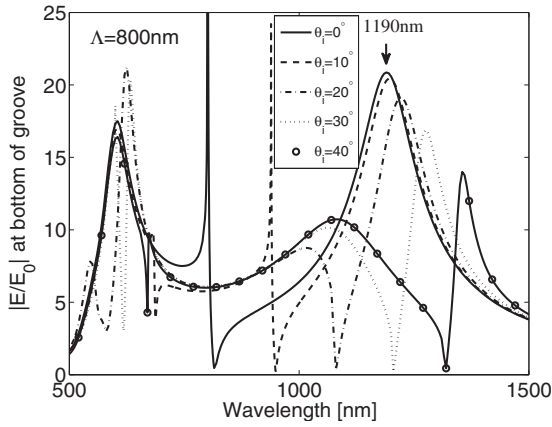


FIG. 6. Enhancement spectra of the electric field magnitude (compared to the incident *p*-polarized plane wave) at a position close to the groove bottom of the 800-nm-period grating for different angles θ_i of light incidence.

dence a spike at the wavelength of 800.8 nm (with magnitude $|E/E_0| \approx 36$), which is practically the same as the wavelength $\lambda = \Lambda = 800$ nm, where the first diffraction order in reflection appears at the grazing angle. Notice that, as the angle of incidence increases, the spike/dip splits up into two spikes/dips at the wavelengths given approximately by the relation $\lambda = \Lambda \pm \Lambda \sin \theta_i$.

It is also seen that the resonance peak positioned for normally incident light at the wavelength 1190 nm moves to longer wavelengths with increasing angle of incidence. However, it is important to notice that when the angle of incidence changes only by 10° the redshift is marginal. This (and other more pronounced) redshift is caused by the interference of the resonance peak at 1190 nm with a dip at $\lambda \approx \Lambda + \Lambda \sin \theta_i$ moving progressively to longer wavelengths with increasing θ_i and suppressing the corresponding part of the resonance peak. For the angle of incidence of 40° , a relatively broad peak appears at the wavelength of ~ 1080 nm. We have considered also larger angles of incidence to see if this peak will eventually move its position to 1190 nm with increasing θ_i and found that this was not the case, e.g., for $\theta_i = 60^\circ$ the position did not change compared with $\theta_i = 40^\circ$. A further increase in the angle of incidence to 70° and 80° results in a blueshift of the peak and a decrease in the resonant field at the bottom of the groove.

The suggested interpretation of sharp resonances implies that similar resonances should be observed for higher diffraction orders as well. Indeed, considering normally incident light and the periods of 800 and 1600 nm, we found that, in both cases, a spike at ~ 800 nm is observed in the field-enhancement spectra (Fig. 7) confirming the nature of these resonances as being associated with Rayleigh anomalies whose positions are given by

$$m\lambda = \Lambda(1 \pm \sin \theta_i), \quad m = 1, 2, \dots \quad (7)$$

The near-field distributions at the spike resonance for both periods [Figs. 8(a) and 8(b)] resemble a standing-wave pattern as could be expected since the just appearing new (first for 800-nm-period grating and second for 1600-nm-period

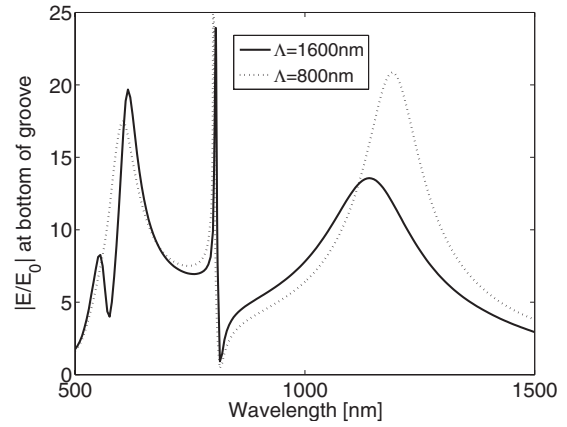


FIG. 7. Electric field-enhancement spectrum (normally incident *p*-polarized light) at a position close to the groove bottom for the 800- and 1600-nm-period groove gratings. The groove height is 200 nm and the groove angle is 20° .

grating) diffraction order is reflected grazing the surface and propagating equally along the positive and negative *x* axis. Note the efficient field excitation inside the grooves at the spike resonances. The corresponding near-field distributions at the wavelength of 815 nm where the electric field enhancement is at a minimum are shown in Figs. 8(c) and 8(d). One notices that the “dip” wavelength is rather close to the light wavelength (~ 816 nm) that can excite the 800-nm-period SPP waves propagating at the air-gold interface. We conjecture therefore that the dips observed at the long-wavelength side of resonant spikes (Figs. 4, 6, and 7) are associated with the diffraction orders giving rise to the SPP excitation with the condition being as follows:

$$m\lambda_{\text{SPP}} = \Lambda(1 \pm \sin \theta_i), \quad m = 1, 2, \dots, \quad (8)$$

where λ_{SPP} is the SPP wavelength at the air-metal interface. Indeed, this hypothesis can also explain the appearance of a small dip at the wavelength of ~ 545 nm in the normal-incidence spectra for the 500-nm-period grating (Figs. 1 and 3) since the SPP wavelength of 500 nm can be excited at ~ 544 nm. It should also be borne in mind that the efficient groove excitation results in a field distribution similar to that of channel plasmon polaritons,¹⁴ which requires in turn the opposite direction of electrical field on the groove sides, a feature that is not compatible with the propagating SPP field distribution. Finally, the near-field distributions at the wavelength of 815 nm [left part of Figs. 8(c) and 8(d)] resemble a standing SPP wave pattern overlaid with another interference pattern—that of normally incident and reflected light. The presence of a SPP wave pattern is more clearly seen in the case where we only show the magnitude of the out-of-plane component (*y*) of the electric field [right part of Figs. 8(c) and 8(d)]. In the case of the period 1600 nm [Fig. 8(d)] we have also shown a cross section of the magnitude of the field (solid curve) together with the magnitude of the field of a SPP (dashed curve). The two curves are practically on top of one another. A similar agreement between the out-of-plane field component and a SPP field was found in the case of Fig. 8(c).

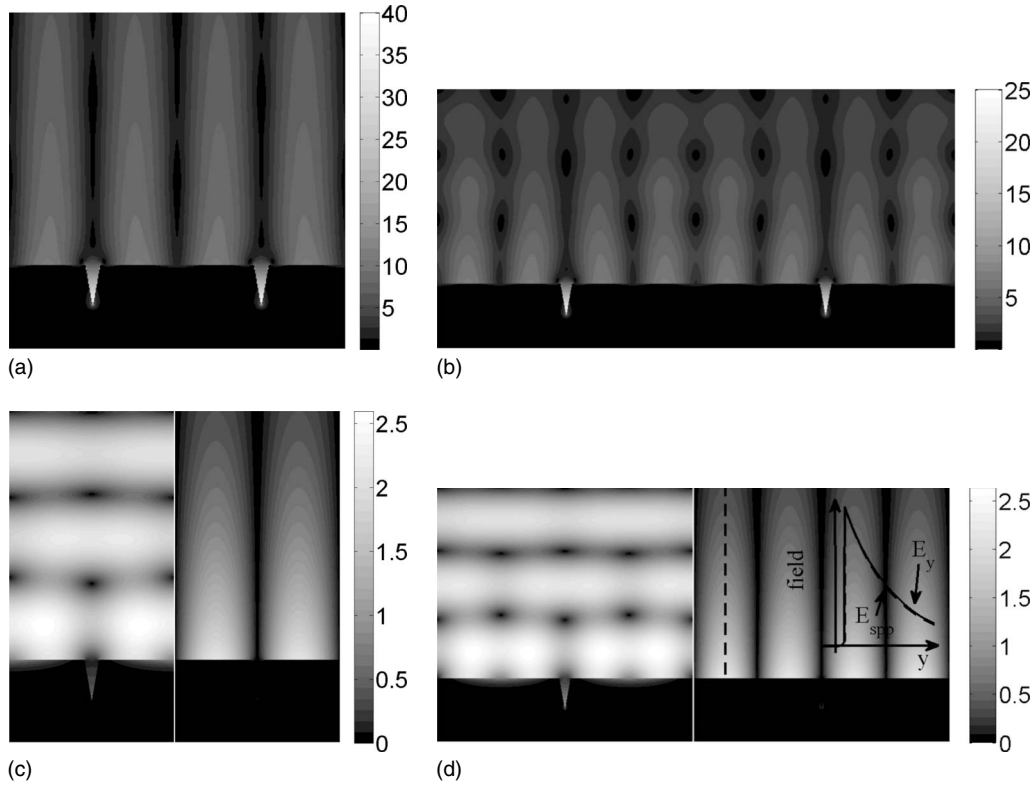


FIG. 8. Normalized electric field magnitude distributions near groove gratings for (a) the period $\Lambda=800$ nm and wavelength $\lambda=800.8$ nm, (b) $\Lambda=1600$ nm and $\lambda=806$ nm, (c) $\Lambda=800$ nm and $\lambda=815$ nm (left part: magnitude of total field, right part: magnitude of out-of-plane field component), and (d) the same as Fig. 8(c) except that the period is $\Lambda=1600$ nm. A cross cut of the field along the dashed line is shown in the inset together with the field magnitude of a SPP. The two curves practically coincide.

The fact that the standing-wave pattern has a node right at the grooves means that the SPP waves will in this case propagate very similar to propagation on a flat surface without grooves, which was actually an assumption in the arguments used to arrive at Eq. (8).

Contrary to the previous case (Fig. 6) the spike for the period 1600 nm is now at a wavelength (806 nm) which is slightly longer compared with the cutoff wavelength of the grating order, although it is just a few nanometers. One could speculate that, for longer periods, the spike and dip conditions [Eqs. (7) and (8)] produce progressively closer wavelengths causing these two phenomena to interfere with each other. At any rate, the near field at the wavelength of the spike resonance [Figs. 8(a) and 8(b)] is not dominated by SPP waves, whose presence is clearly seen at the wavelength of the dip [Figs. 8(c) and 8(d)]. This is seen by noticing that the field is shown for distances up to 1200 nm above the grating surface and that the field magnitude of the flat-gold-surface SPP should decrease by a factor $1/e$ within the distance of 623 nm for the wavelengths close to 800 nm.

V. SCALING OF THE GROOVE PERIODICITY

The above interpretation of the long-wavelength resonance (identified first in Fig. 1) as being due to the SPP reflection by the neighbor grooves implies that the resonance position (being determined by the SPP round-trip propagation) should not be changed when the grating period is

changed by an integer number of half-SPP wavelengths. In order to check this feature, let us consider, as a starting point, the period 1600 nm, in which case there is a field-enhancement resonance peak at the wavelength 1140 nm (Fig. 7), and increase or decrease the period by an integer number of half-SPP wavelengths at resonance ($\lambda_{SPP} \approx 1130$ nm). The simulation results shown in Fig. 9 demonstrate clearly that changing the groove period by a half of the SPP wavelength results in a structure with the resonance at (approximately) the same wavelength. Note that, for the pe-

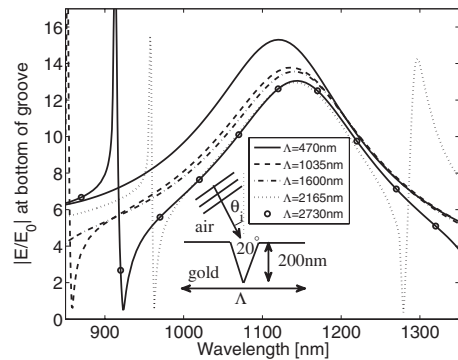


FIG. 9. Field-enhancement spectra for groove gratings where the periods differ by an integer number of half-SPP wavelengths at resonance. For the periods $\Lambda=470$, 1600, and 2730 nm the angle of incidence is $\theta_i=0^\circ$. For the periods $\Lambda=1035$ and 2165 nm the angle of incidence is $\theta_i=40^\circ$ and 50° , respectively.

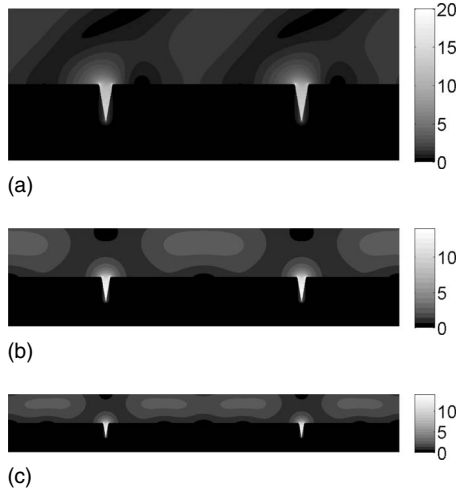


FIG. 10. Normalized electric field magnitude distributions at the resonant wavelength of ~ 1130 nm for groove gratings with (a) period $\Lambda=1035$ nm and angle of incidence $\theta_i=40^\circ$, (b) $\Lambda=1600$ nm, $\theta_i=0^\circ$, and (c) $\Lambda=2730$ nm, $\theta_i=0^\circ$. The groove height is 200 nm and the groove angle is 20° .

periods $\Lambda=470, 1600,$ and 2730 nm we considered the normal incidence, $\theta_i=0^\circ$. For the other periods, $\Lambda=1035$ and 2165 nm, the resonance peak does not appear for the case of normally incident light, which can be explained by the symmetry mismatch between incident and resonant fields. Considering, e.g., the incident magnetic field, or the x component of the electric field, the even symmetry of these field components in one period of the structure is not broken because the structure within the period is symmetric. Thus the resulting total fields will also be of even symmetry, and consequently resonant fields with odd symmetry cannot be excited with normally incident light. Furthermore, the resonance peak can also be modified due to interference with the Rayleigh anomaly, and the appropriate angle of light incidence must be chosen in a way so that the Rayleigh anomaly, i.e., the wavelengths given by Eqs. (7) and (8), are not too close to the resonance peak. For the structures with periods $\Lambda=1035$ and 2165 nm the resonances appear for the angles of incidence $\theta_i=40^\circ$ ($\Lambda=1035$ nm) and $\theta_i=50^\circ$ ($\Lambda=2165$ nm), when the Rayleigh anomaly is moved sufficiently far away.

The corresponding resonant near-field distributions show features confirming the excitation of first-order to fifth-order standing waves (Fig. 10). The resonant field distribution for the period of 470 nm (not shown) is very similar to that displayed in Fig. 2(b) with one node (minimum) in the field being located at the surface in the middle between the grooves. The field distribution at the second-order resonance [Fig. 10(a)] features correspondingly two nodes, that at the third-order resonance [Fig. 10(b)] three nodes, and so on [Fig. 10(c)].

We conclude this section by considering another resonance, namely, the long-wavelength resonance shown in Fig. 6 (period $\Lambda=800$ nm) at the wavelength of 1190 nm for the normally incident light. In this case as well, increasing the period by a half of SPP wavelength ($\lambda_{\text{spp}} \approx 1180$ nm) results in a structure with the resonance at the same wavelength, if

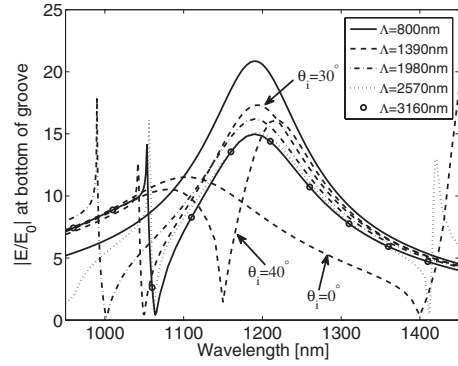


FIG. 11. Field-enhancement spectra for groove gratings where the periods differ by an integer number of half-SPP wavelengths at resonance. For the periods $\Lambda=800, 1980,$ and 3160 nm the angle of incidence is $\theta_i=0^\circ$. For the period $\Lambda=2570$ nm the angle of incidence is $\theta_i=40^\circ$, and for $\Lambda=1390$ nm we consider the three angles of incidence $\theta_i=0^\circ, \theta_i=30^\circ,$ and $\theta_i=40^\circ$.

the angle of incident light is chosen appropriately (Fig. 11). In this case, three spectra for the period of 1390 nm corresponding to three different angles of incident light are shown. For the angle of incidence 30° the resonance peak at wavelength ~ 1190 nm appears. However, when this angle is 40° the Rayleigh anomaly is located very close to the resonance wavelength and the resonance peak is modified. For the case of normally incident light the structure with period 1390 nm has a Rayleigh anomaly at the wavelength ~ 1400 nm similar to the case of the structure with period 2570 nm. In the latter case (period 2570 nm) this anomaly does not lead to modification of the resonance peak at wavelength ~ 1190 nm, and so it is also not obvious that this anomaly could be an alternative explanation of why the resonance does not appear at the wavelength ~ 1190 nm for the period 1390 nm and normal light incidence. However, in this case the resonance cannot be excited with normally incident light for symmetry reasons.

VI. REFLECTION SPECTRA

Finally, we shall take a closer look at reflection spectra for the case of normally incident light for groove-grating structures with a number of different periods. In Fig. 12 we have presented field-enhancement spectra [Fig. 12(a)] and corresponding reflection spectra [Fig. 12(b)]. Clearly, the wavelength of the short-wavelength resonance peak that we saw in Fig. 2(a), which was localized to the bottom of the groove, does not change much when changing the period, as far as the field-enhancement spectrum is concerned. On the other hand the standing-wave resonance [e.g., Fig. 2(b)] redshifts with increasing period, which is consistent with the interpretation of this resonance as being related to SPPs propagating back and forth between grooves. For the larger periods we notice the appearance of a spike similar to those considered previously. When this spike is close to the groove resonance [Fig. 2(a)] it looks as if the field-enhancement peak is split into two peaks. The redshifting of the standing-wave resonance with increasing period is also clearly observed in the

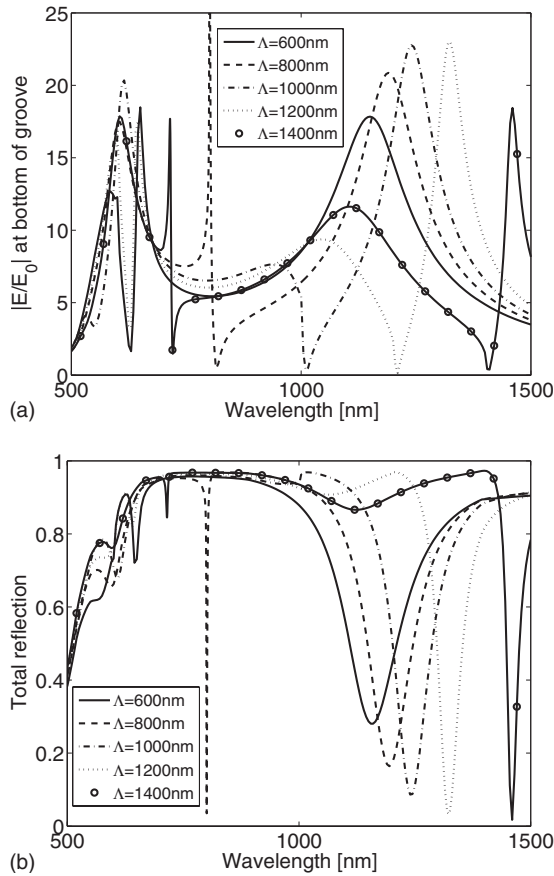


FIG. 12. (a) Electric field-enhancement spectra (normally incident p -polarized light) at a position close to the bottom of the periodically repeated groove (period Λ). The groove height is 200 nm and the groove angle is 20° . (b) Reflection spectra including all grating-reflection orders for the same gratings.

reflection spectrum considering reflection into all orders [Fig. 12(b)]. Notice the close match between peaks, including spikes, in field-enhancement spectra and dips in corresponding reflection spectra. The minimum in field enhancement for $\Lambda=1000$ nm shows up in reflection as a small sudden increase with wavelength.

In order to measure the total reflection it is necessary to integrate over light propagating in all reflection directions. In the calculation we only have to sum over the discrete directions corresponding to the reflection-grating orders. In a measurement where reflection is only measured for a specific direction, e.g., zero-order reflection (going directly upward here), the measured reflection will differ significantly from the total reflection if the period is large enough (or the wavelength small enough) that the grating supports higher-order reflection. In Fig. 13 we consider the zero-order and first-order reflection separately. Notice that the zero-order reflection spectrum (Fig. 13) can have some very large extra reflection dips compared to the total reflection [Fig. 12(b)]. However, when summing over all the reflection orders some of these reflection dips in the spectrum completely disappear since the reflection dip in the zero-order reflection matches the reflection increase in the first-order reflection. Also note that the first, second, third... orders have a cutoff wavelength

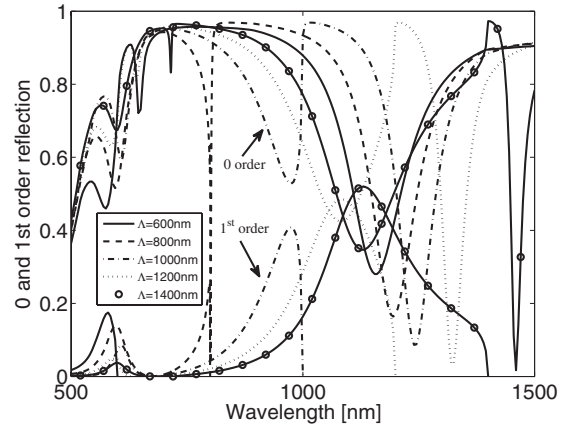


FIG. 13. Zero-order and first-order reflection spectra for the same structures considered in Fig. 12.

where reflected light will be grazing the grating surface. Changing the wavelength for the higher orders changes the reflection angle making the measurement of the spectrum more difficult compared with zero-order reflection.

We should mention that for a related structure with a periodic arrangement of metal nanowires placed on top of an indium-tin-oxide (ITO) waveguide layer it has been experimentally observed that extinction maxima redshift with increasing period between nanowires [similar to the observation in Fig. 12(a)], and that extinction minima for the angle of light incidence 0° can split up into two minima with increasing angle of light incidence, which we observed in Fig. 6 and described by Eq. (8).⁴⁰ In the case of Ref. 40 light is transported from one wire to the next via the ITO waveguide layer whereas in our case light is transported from one groove to the next via the metal surface acting as a waveguide for SPP waves. For a 2D array of nanorods it has also been experimentally observed that a transmission minimum redshifts with increased pitch between the rods.⁴¹

VII. CONCLUSION

In conclusion, we have considered the optical properties of triangular-groove gold gratings characterized by groove height, groove angle, and the period between grooves. If the grating period is smaller than the wavelength (normally incident light) we typically find only two resonances. The first resonance at wavelengths of approximately 600–700 nm is determined by the geometry of individual grooves, namely, groove height and groove angle. The resonance blueshifts slightly with increasing groove angle and redshifts with increasing height. In one case the local enhancement of the electric field magnitude near the bottom of the groove for one of these resonances reached a factor of 35. We also find another resonance at larger wavelengths that can be explained as a standing-wave resonance due to SPPs being reflected back and forth between neighbor grooves. This explanation was supported by showing that the resonance wavelength redshifts with increasing period and increasing groove height, and geometries with a resonance at the same wavelength can be constructed by increasing the period by

an integer number of half-SPP wavelengths. Furthermore, the resonance is not sensitive to the angle of incident light (except if there is another important resonance present), and calculated resonant fields show an integer number of nodes in the near-field close to the surface and between grooves matching the order of the standing-wave resonance.

For structures with longer periods exceeding the wavelengths considered, or when we use oblique angles of incidence, we found the appearance of a spike (Rayleigh anomaly) in the field-enhancement spectrum at wavelengths close to the cutoff wavelength of a higher-order reflection from the grating. For a short period (800 nm) the spike wavelength was at this precise cutoff wavelength within 1 nm but for the period 1600 nm the spike wavelength was longer than half the period by 6 nm. We can try to explain this in the way that the spike is affected by SPP waves to a larger extent for the larger periods.

We have shown that the resonances are observable in reflection spectra. The best correspondence between reflection dips and local-field-enhancement peaks due to various resonances is obtained by considering the total reflection into all grating-reflection orders. If the grating period is larger than the wavelength there will be higher-order reflection, in which case there will be additional reflection minima in the more easily measurable zero-order reflection compared to the total reflection.

Finally, we have seen that by varying the periodicity, groove height, and angle, the standing-wave resonances observed in near-field spectra and reflection spectra can be tuned within a wide range of wavelengths from the visible to the infrared, which makes the grating configuration interesting for, e.g., sensing and surface-enhanced spectroscopies.

*ts@nano.aau.dk

- ¹ *Surface Plasmon Nanophotonics*, edited by M. L. Brongersma and P. G. Kik (Springer, New York, 2007).
- ² *Plasmonic Nanoguides and Circuits*, edited by S. I. Bozhevolnyi (Pan Stanford, Singapore, 2009).
- ³ H. R  ther, *Surface Plasmons* (Springer, New York, 1988).
- ⁴ G. L  v  que and O. J. F. Martin, *J. Appl. Phys.* **100**, 124301 (2006).
- ⁵ J. Renger, S. Grafstr  m, and L. M. Eng, *Phys. Rev. B* **76**, 045431 (2007).
- ⁶ H. Hori, K. Tawa, K. Kintaka, J. Nishi, and Y. Tatsu, *Opt. Rev.* **16**, 216 (2009).
- ⁷ E. Popov, N. Bonod, and S. Enoch, *Opt. Express* **15**, 4224 (2007).
- ⁸ I. P. Radko, S. I. Bozhevolnyi, G. Bruccoli, L. Mart  n-Moreno, F. J. Garc  a-Vidal, and A. Boltasseva, *Phys. Rev. B* **78**, 115115 (2008).
- ⁹ F. L  pez-Tejiera, F. J. Garc  a-Vidal, and L. Mart  n-Moreno, *Phys. Rev. B* **72**, 161405(R) (2005).
- ¹⁰ T. S  ndergaard, S. I. Bozhevolnyi, and A. Boltasseva, *Phys. Rev. B* **73**, 045320 (2006).
- ¹¹ J. A. S  nchez-Gil, *Opt. Lett.* **32**, 2330 (2007).
- ¹² T. W. Ebbesen, H. J. Lezec, H. F. Ghaemi, T. Thio, and P. A. Wolff, *Nature (London)* **391**, 667 (1998).
- ¹³ F. J. Garc  a-Vidal, H. J. Lezec, T. W. Ebbesen, and L. Mart  n-Moreno, *Phys. Rev. Lett.* **90**, 213901 (2003).
- ¹⁴ S. I. Bozhevolnyi, V. S. Volkov, E. Devaux, J.-Y. Laluet, and T. W. Ebbesen, *Nature (London)* **440**, 508 (2006).
- ¹⁵ E. Moreno, F. J. Garc  a-Vidal, S. G. Rodrigo, L. Mart  n-Moreno, and S. I. Bozhevolnyi, *Opt. Lett.* **31**, 3447 (2006).
- ¹⁶ D. F. P. Pile and D. K. Gramotnev, *Opt. Lett.* **29**, 1069 (2004).
- ¹⁷ J. Dintinger and O. J. F. Martin, *Opt. Express* **17**, 2364 (2009).
- ¹⁸ R. B. Nielsen, I. Fernandez-Cuesta, A. Boltasseva, V. S. Volkov, S. I. Bozhevolnyi, A. Klukowska, and A. Kristensen, *Opt. Lett.* **33**, 2800 (2008).
- ¹⁹ A. Hessel and A. A. Oliner, *Appl. Opt.* **4**, 1275 (1965).
- ²⁰ R. W. Wood, *Philos. Mag.* **4**, 396 (1902).
- ²¹ V. G. Kravets, F. Schedin, and A. N. Grigorenko, *Phys. Rev. Lett.* **101**, 087403 (2008).
- ²² T. L  pez-Rios, D. Mendoza, F. J. Garc  a-Vidal, J. S  nchez-Dehesa, and B. Pannetier, *Phys. Rev. Lett.* **81**, 665 (1998).
- ²³ F. J. Garc  a-Vidal *et al.*, *J. Lightwave Technol.* **17**, 2191 (1999).
- ²⁴ M. Kuttge, E. J. R. Vesseur, and A. Polman, *Appl. Phys. Lett.* **94**, 183104 (2009).
- ²⁵ P. M  hlschlegel, H.-J. Eisler, O. J. F. Martin, B. Hecht, and D. W. Pohl, *Science* **308**, 1607 (2005).
- ²⁶ L. Novotny, *Phys. Rev. Lett.* **98**, 266802 (2007).
- ²⁷ T. S  ndergaard and S. I. Bozhevolnyi, *Phys. Status Solidi B* **245**, 9 (2008).
- ²⁸ T. S  ndergaard, J. Beermann, A. Boltasseva, and S. I. Bozhevolnyi, *Phys. Rev. B* **77**, 115420 (2008).
- ²⁹ Y. Kurokawa and H. T. Miyazaki, *Phys. Rev. B* **75**, 035411 (2007).
- ³⁰ K. Imura, T. Nagahara, and H. Okamoto, *J. Chem. Phys.* **122**, 154701 (2005).
- ³¹ H. Ditlbacher, A. Hohenau, D. Wagner, U. Kreibig, M. Rogers, F. Hofer, F. R. Aussenegg, and J. R. Krenn, *Phys. Rev. Lett.* **95**, 257403 (2005).
- ³² F. Neubrech, T. Kolb, R. Lovrincic, G. Fahsold, A. Pucci, J. Aizpurua, T. W. Cornelius, M. E. Toimil-Molares, R. Neumann, and S. Karim, *Appl. Phys. Lett.* **89**, 253104 (2006).
- ³³ T. Laroche and C. Girard, *Appl. Phys. Lett.* **89**, 233119 (2006).
- ³⁴ P. B. Johnson and R. W. Christy, *Phys. Rev. B* **6**, 4370 (1972).
- ³⁵ T. S  ndergaard, *Phys. Status Solidi B* **244**, 3448 (2007).
- ³⁶ D. W. Prather, M. S. Mirotznik, and J. N. Mait, *J. Opt. Soc. Am. A Opt. Image Sci. Vis.* **14**, 34 (1997).
- ³⁷ J. Jin, *The Finite Element in Electromagnetics* 2nd ed. (John Wiley & Sons, New York, 2002).
- ³⁸ G. Kobidze, B. Shanker, and D. P. Nyquist, *Phys. Rev. E* **72**, 056702 (2005).
- ³⁹ D. Van Orden and V. Lomakin, *IEEE Trans. Antennas Propag.* **57**, 1973 (2009).
- ⁴⁰ A. Christ *et al.*, *Phys. Rev. Lett.* **91**, 183901 (2003).
- ⁴¹ B. Augu  ie and W. L. Barnes, *Phys. Rev. Lett.* **101**, 143902 (2008).